# Giant Nonlinear Photon-Drag Currents in Centrosymmetric Moiré Bilayers

Zhuocheng Lu,<sup>1,\*</sup> Zhuang Qian,<sup>2,\*</sup> Zhichao Guo,<sup>1</sup> Likun Shi,<sup>1</sup> Shi Liu,<sup>2</sup> Hua Wang,<sup>1,†</sup> and Kai Chang<sup>1,‡</sup>

<sup>1</sup> Center for Quantum Matter, School of Physics, Zhejiang University, Zhejiang 310058, China

<sup>2</sup> Department of Physics, School of Science, Westlake University, Hangzhou, Zhejiang 310030, China

We present a unified microscopic theory of nonlinear photon-drag currents, formulated within a geometric-loop framework that provides both transparent quantum-geometric interpretation and numerical tractability. In this picture, the photon-drag shift current corresponds to the dipole moment of the geometric loop, while the photon-drag injection current arises from the same loop weighted by a band velocity difference. We apply the theory to an exact continuum model of twisted bilayer graphene (TBG) with *ab initio* accuracy. Remarkably, an in-plane wavevector only a few times larger than that of free-space photons already produces sizable photon-drag currents in centrosymmetric TBG, comparable to photogalvanic responses in typical noncentrosymmetric two-dimensional materials. These currents are broadly tunable by twist angle, photon wavevector, and light polarization. Our results establish a quantum geometric framework for nonlinear photon-drag phenomena and highlight moiré bilayers as promising platforms for large, highly tunable optoelectronic responses.

Introduction.—Second-order photogalvanic responses have garnered sustained interest as powerful probes of symmetry and band geometry in quantum materials [1– 11]. However, this nonlinear dc photocurrent vanishes in centrosymmetric crystals because inversion symmetry forbids any preferred current direction. This limitation can be remedied by accounting for momentum transfer from photons to carriers, but the resulting photondrag effect is typically negligible since free-space photons carry little momentum. The situation changes when the light field is engineered to enhance momentum transfer. Structured beams with spatially varying phase and amplitude, such as tightly focused Gaussian beams, reduce spatial symmetry and effectively supply large momenta through spatial dispersion, enabling measurable photogalvanic signals [12]. Polaritonic confinement provides a complementary route: subwavelength surface plasmons and related polaritons compress optical wavelengths by tens to hundreds of times, generating large wavevectors and intense near-field gradients that can amplify photondrag by orders of magnitude [13–15]. These developments demonstrate that enhanced photon-drag can circumvent symmetry constraints and unlock new regimes of nonlinear optoelectronic response.

Despite early progress establishing photon-drag injection and shift currents as the dominant contributions to nonlinear photon-drag responses, only limited toy-model analyses exist [16, 17]. A key challenge is computing the nonlinear photon-drag shift current in real materials: physically transparent formulations rely on gauge-dependent quantities (e.g., Berry connections), hindering stable numerical evaluation, whereas gauge-invariant sum-rule expressions obscure the underlying quantum geometry by involving contributions from all remote bands. Compounding these challenges, photon-drag phenomena

in emerging quantum materials remain largely unexplored. Among them, twisted bilayer graphene (TBG) stands out as a tunable moiré platform with flat bands and a rich landscape of correlated and topological phases [18–25]. While intrinsic TBG is centrosymmetric and exhibits no photogalvanic effect under uniform illumination, its enlarged moiré supercell significantly compresses the Brillouin zone, making even modest photon wavevectors comparable to a significant portion of the zone. Consequently, photon-drag can generate sizable nonlinear currents, positioning TBG as an ideal system for systematic exploration.

In this work, we develop a geometric-loop formalism for nonlinear photon-drag currents that unifies the injection and shift contributions within a single, transparent framework, enabling both conceptual clarity and robust numerical implementation. We derive symmetry constraints on the nonlinear photon-drag photoconductivity tensor and apply the theory to TBG using an exact continuum model with ab initio level precision. Our calculations reveal remarkably large photon-drag responses, comparable to the giant photogalvanic effects predicted for typical noncentrosymmetric two-dimensional materials. We further characterize their scaling with photon wavevector and their twist-angle dependence. Finally, we analyze TBG aligned with hexagonal boron nitride, where inversion breaking restores a conventional photogalvanic response. Distinct magnitudes and k-space textures clearly separate the mechanisms of wavevectorindependent and photon-drag contributions.

Geometric loop formalism.—We now develop a geometric-loop formulation of the nonlinear photon-drag current, a photogalvanic response in which finite-momentum photoexcitation is essential, as schematized in Fig. 1(a). The inhomogeneous electric field responsible for this effect is given by  $\mathbf{E}(\mathbf{r},t) = \mathbf{E}(\omega)e^{i\mathbf{q}\cdot\mathbf{r}-i\omega t} + c.c.$ , where  $\mathbf{q}$  is the wavevector, and  $\omega$  is the frequency. From the density-matrix derivation, the total nonlinear photon-drag current density,  $J^{a,(2)}$  then can be written

<sup>\*</sup> These authors contributed equally to this work.

<sup>†</sup> daodaohw@zju.edu.cn

<sup>&</sup>lt;sup>‡</sup> kchang@zju.edu.cn

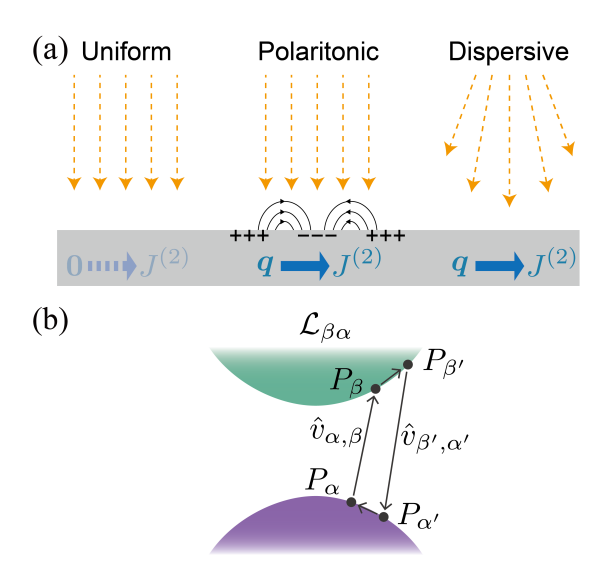


FIG. 1. (a) Uniform illumination yields no photogalvanic current in a centrosymmetric medium, whereas finite q produces a nonlinear photon-drag current  $J^{(2)}$  via polaritonic enhancement or spatially dispersive beams. (b) Schematic of the geometric loop  $\mathcal{L}_{\beta\alpha}$ . The loop connects four Bloch states  $\alpha, \beta, \alpha', \beta'$ , with  $\alpha, \alpha'$  in the valence band and  $\beta, \beta'$  in the conduction band. The momenta of  $\alpha, \beta, \alpha', \beta'$  are related by  $\mathbf{k}_{\beta} - \mathbf{k}_{\alpha} = \mathbf{k}_{\beta'} - \mathbf{k}_{\alpha'} = \mathbf{q}$  and  $\mathbf{k}_{\beta'} - \mathbf{k}_{\beta} = \mathbf{k}_{\alpha'} - \mathbf{k}_{\alpha} = \mathbf{p}$ , where  $\mathbf{p}$  is an infinitesimal displacement.

as [26]:

$$J^{a,(2)} = \left(\sigma_{\rm IC}^{abc} + \sigma_{\rm SC}^{abc}\right) E_b(\omega) E_c(-\omega), \tag{1}$$

where  $\sigma_{\rm IC}^{abc}$  represents the injection current, while  $\sigma_{\rm SC}^{abc}$  accounts for the shift current. For brevity, the  $\boldsymbol{q}$  and  $\omega$  dependences of J and  $\sigma$  are suppressed. The summation over the Cartesian indices is implied.

The photon-drag injection-current photoconductivity  $\sigma^{abc}_{IC}$  can be expressed as

$$\sigma_{\rm IC}^{abc} = 2\tau \mathcal{C} \sum_{n_{\alpha}, n_{\beta}, \mathbf{k}} \mathcal{J}_{\alpha\beta}(\omega) \left( v_{\beta\beta}^{a} - v_{\alpha\alpha}^{a} \right) v_{\beta\alpha}^{b} v_{\alpha\beta}^{c}, \qquad (2)$$

where  $\tau$  is the relaxation time,  $\mathcal{C} = \pi e^3/\hbar^2 \omega^2$ ,  $\sum_{\mathbf{k}}$  indicates  $\int d^d k/(2\pi)^d$ . The composite indices  $\alpha = (n_{\alpha}, \mathbf{k}_{\alpha})$  and  $\beta = (n_{\beta}, \mathbf{k}_{\beta})$  refer to states before and after photoexcitation, with  $\mathbf{k}_{\alpha} = \mathbf{k} - \mathbf{q}/2$ ,  $\mathbf{k}_{\beta} = \mathbf{k} + \mathbf{q}/2$ .  $\mathcal{J}_{\alpha\beta}(\omega) = (f_{\alpha} - f_{\beta}) \, \delta(\omega_{\beta} - \omega_{\alpha} - \omega)$  is the joint density of states, representing the nonvertical transitions of energy  $\hbar \omega$  from state  $\alpha$  to  $\beta$ . The velocity matrix elements are given by  $v_{\alpha\beta}^b = \langle u_{\alpha} | \hat{v}_{\alpha,\beta}^b | u_{\beta} \rangle$ , where the velocity operator is  $\hat{v}_{\alpha,\beta}^b \equiv \frac{1}{2} (\hat{v}_{\mathbf{k}_{\alpha}}^b + \hat{v}_{\mathbf{k}_{\beta}}^b)$ .

The photon-drag shift-current photoconductivity  $\sigma_{\rm SC}^{abc}$  is given by

$$\sigma_{\rm SC}^{abc} = \mathcal{C} \sum_{n_{\alpha}, n_{\beta}, \mathbf{k}} \mathcal{J}_{\alpha\beta}(\omega) \left( R_{\beta\alpha}^{b;a} - R_{\alpha\beta}^{c;a} \right) v_{\beta\alpha}^{b} v_{\alpha\beta}^{c}, \tag{3}$$

where the shift vector is

$$R_{\beta\alpha}^{b;a} = i\partial_{k^a} \log v_{\beta\alpha}^b + r_{\beta\beta}^a - r_{\alpha\alpha}^a, \tag{4}$$

with  $r^a_{\alpha\alpha}$  denoting the Berry connection. Eq. (3) admits a transparent interpretation: it is the wavepacket shift between conduction and valence bands,  $R^{b;a}_{\beta\alpha}$ , weighted by the velocity matrix elements  $v^c_{\alpha\beta}v^b_{\beta\alpha}$  and the joint density of states  $\mathcal{J}_{\alpha\beta}(\omega)$ . Although  $R^{b;a}_{\beta\alpha}$  is gauge-invariant, it is built from the derivative of the gauge-dependent velocity matrix, and therefore, not directly amenable to numerical evaluation. Alternatively, one can use the sum-rule expression:

$$iR^{b;a}_{\beta\alpha}v^b_{\beta\alpha} = -w^{ba}_{\beta\alpha} + \sum_{n_{\alpha} \neq n_{\beta}} \frac{v^a_{\beta\gamma}v^b_{\gamma\alpha}}{\omega_{\gamma\beta}} - \sum_{n_{\alpha} \neq n_{\alpha}} \frac{v^b_{\beta\gamma}v^a_{\gamma\alpha}}{\omega_{\alpha\gamma}}, \tag{5}$$

where  $w_{\alpha\beta}^{ca} = \langle u_{\alpha} | \partial_{k^a} v_{\alpha,\beta}^c | u_{\beta} \rangle$  the inverse effective mass matrix. While Eq. (5) is numerically tractable, it masks the underlying quantum-geometric interpretation and physics, as it entails sums over multiple terms and intermediate bands.

To combine geometric transparency with numerical efficiency, we derive alternative expressions for the shift and injection contributions to the photon-drag response. Before introducing the recast form, we define the geometric loop as

$$\mathcal{L}_{\beta\alpha}^{abc}(p) = \langle P_{\beta'} \hat{v}_{\beta',\alpha'}^b P_{\alpha'} P_{\alpha} \hat{v}_{\alpha,\beta}^c P_{\beta} \rangle_{\beta}, \tag{6}$$

with  $\alpha=(n_{\alpha},\boldsymbol{k}_{\alpha}),\ \alpha'=(n_{\alpha},\boldsymbol{k}_{\alpha}+p\hat{\boldsymbol{a}}),\ \beta=(n_{\beta},\boldsymbol{k}_{\beta}),\ \beta'=(n_{\beta},\boldsymbol{k}_{\beta}+p\hat{\boldsymbol{a}}),$  where p is an infinitesimal displacement  $(p\to 0^+),\ \hat{\boldsymbol{a}}$  is the unit vector along Cartesian direction  $a,\ P_{\alpha}=|u_{\alpha}\rangle\langle u_{\alpha}|$  is the quantum-state projector and  $\langle\ldots\rangle_{\alpha}$  denotes  $\langle u_{\alpha}|\ldots|u_{\alpha}\rangle$ .  $\mathcal{L}_{\beta\alpha}^{abc}(p)$  is built as a concatenation of quantum-state projectors and velocity operators, forming a geometric loop that connects the valence and conduction band states. The geometric loop defined by  $\mathcal{L}_{\beta\alpha}^{abc}(p)$  is illustrated in Fig. 1(b).

Rewriting the photon-drag shift-current photoconductivity in terms of  $\mathcal{L}_{\beta\alpha}^{abc}\left(p\right)$  yields

$$\sigma_{\rm SC}^{abc} = \mathcal{C} \sum_{p, n, \alpha, k} \mathcal{J}_{\alpha\beta}(\omega) \left( \hat{D}_p \mathcal{L}_{\beta\alpha}^{abc}(p) - \hat{D}_p \mathcal{L}_{\alpha\beta}^{acb}(p) \right), \quad (7)$$

where  $\hat{D}_p = i\partial_p$  is the dipole operator [27]. In this representation the velocity product and shift vector in Eq. (3) are expressed as  $v^b_{\beta\alpha}v^c_{\alpha\beta} = \mathcal{L}^{abc}_{\beta\alpha}(p)$  and  $R^{b;a}_{\beta\alpha} = \hat{D}_p \log \mathcal{L}^{abc}_{\beta\alpha}(p)$ . Eq. (7) indicates that the quantum-geometric content of  $\sigma^{abc}_{\rm SC}$  is encoded in the dipole of the geometric loop. Because  $\mathcal{L}^{abc}_{\beta\alpha}(p)$  is gauge invariant, that derivative can be obtained numerically via finite differences. Using the same strategy, the photon-drag injection-current photoconductivity becomes

$$\sigma_{\rm IC}^{abc} = 2\tau \mathcal{C} \sum_{n_{\alpha}, n_{\beta}, \mathbf{k}} \mathcal{J}_{\alpha\beta}(\omega) \left( v_{\beta\beta}^{a} - v_{\alpha\alpha}^{a} \right) \mathcal{L}_{\beta\alpha}^{abc}(p). \tag{8}$$

In this formulation, the quantum-geometric origin of  $\sigma_{\rm IC}^{abc}$  is captured by  $\mathcal{L}_{\beta\alpha}^{abc}(p)$ , weighted by the velocity difference between the conduction and valence bands.

Symmetry perspective.—Inversion  $(\mathcal{P})$  and time reversal  $(\mathcal{T})$  are fundamental symmetries of quantum materials. Here we derive how  $\mathcal{P}, \mathcal{T}$  and their combinations constrain  $\sigma_{\text{IC}}^{abc}$  and  $\sigma_{\text{SC}}^{abc}$ . We begin by expanding the response in powers of the photon wavevector,

$$\sigma^{abc}(\mathbf{q}) = \sigma^{abc} + q_d \, \sigma^{abcd} + q_d q_e \, \sigma^{abcde} + \cdots, \qquad (9)$$

where the expansion coefficients  $\sigma^{abc}$ ,  $\sigma^{abcd}$ ,  $\sigma^{abcde}$ , ... are independent of  $\boldsymbol{q}$ . Noting that  $\boldsymbol{q}$  is an external parameter characterizing the light field and is odd under  $\mathcal{P}$  and  $\mathcal{T}$ , we therefore decompose the response into parts even and odd in  $\boldsymbol{q}$ :

$$\sigma^{abc}(\mathbf{q}) = \sigma^{abc}(\mathbf{q}_{\text{even}}) + \sigma^{abc}(\mathbf{q}_{\text{odd}}), \tag{10}$$

where  $\sigma^{abc}(\boldsymbol{q}_{\mathrm{even}})$  is dominated by the homogeneous contribution  $(\boldsymbol{q}^0)$ , whereas the leading contribution for  $\sigma^{abc}(\boldsymbol{q}_{\mathrm{odd}})$  are the injection-current and shift-current dipoles  $(\boldsymbol{q}^1)$ . The resulting symmetry constraints for  $\sigma^{abc}_{\mathrm{IC}}$  and  $\sigma^{abc}_{\mathrm{SC}}$  under  $\mathcal{P}$ ,  $\mathcal{T}$ , and  $\mathcal{P}\mathcal{T}$  are summarized in Table I [28].

TABLE I. Allowed components of  $\sigma_{\rm IC}^{abc}$  and  $\sigma_{\rm SC}^{abc}$  under the following symmetries:  $\mathcal{P}$  (inversion),  $\mathcal{T}$  (time-reversal),  $\mathcal{PT}$  (space-time inversion), and both  $\mathcal{P}$  and  $\mathcal{T}$ . Columns labeled  $q_{\rm even}$  and  $q_{\rm odd}$  list responses even/odd in the photon wavevector. Labels L/C mark the linear (real) and circular (imaginary) parts as even under the listed symmetry; absence of a label indicates an odd part. The symbol  $\times$  marks cases where both linear and circular parts are odd.

Symmetry	$\sigma^{abc}_{ m IC}(m{q}_{ m even})$	$\sigma^{abc}_{ m IC}(m{q}_{ m odd})$	$\sigma^{abc}_{ m SC}(oldsymbol{q}_{ m even})$	$\sigma^{abc}_{ m SC}(m{q}_{ m odd})$
$\mathcal{P}$	×	L,C	×	L,C
${\mathcal T}$	$\mathbf{C}$	$_{\rm L}$	${ m L}$	$^{\mathrm{C}}$
$\mathcal{P}\mathcal{T}$	${ m L}$	${ m L}$	$^{\mathrm{C}}$	$^{\mathrm{C}}$
$\mathcal{P}\&\mathcal{T}$	×	${ m L}$	×	$^{\mathrm{C}}$

Twisted bilayer graphene.—Motivated by the moiré enhancement of photon-drag effects, we use TBG as a case study. We employ an exact continuum model based on the ab initio informed framework of Carr et al. [29]. Relative to the well-known Bistritzer-MacDonald model [30], this model incorporates three essential improvements: (i) atomic relaxation taken from elastic-theory-relaxed geometries, including in-plane strain and out-of-plane corrugation: (ii) moiré couplings beyond the first shell, necessary to capture stacking-order variations at small angles; and (iii) explicit k-dependent terms that enable the  $k \cdot p$  model to reproduce more accurately the particlehole asymmetry of realistic ab initio bands. Within this framework, relaxation narrows and shifts the magic-angle window toward  $\sim 1^{\circ}$  and removes the spurious "second" magic angle found in unrelaxed models. The continuum couplings are obtained by fitting to density-functionalbased tight-binding supercells over  $0.18^{\circ} < \theta < 6^{\circ}$ , which preserves first-principles accuracy while allowing smooth interpolation in  $\theta$ . The combination of fidelity and efficiency makes this continuum model a practical backbone

for our investigation of the nonlinear photon-drag currents in TBG. We note that the continuum model treats only a single valley K; the K' contribution follows from time reversal. According to Table I, the total response for the  $\mathcal{T}$ -symmetric TBG is

$$\sigma_{\text{cmp},K+K'}^{abc}(\boldsymbol{q}_{\text{even/odd}}) = \sigma_{\text{cmp},K}^{abc}(\boldsymbol{q}) \pm \sigma_{\text{cmp},K}^{abc}(-\boldsymbol{q}),$$
 (11)

with "+" for the **q**-even components (cmp = IC, C or SC, L) and "–" for the **q**-odd components (cmp = IC, L or SC, C). Moreover, in centrosymmetric TBG, the additional  $\mathcal P$  eliminates all **q**-even contributions, leaving the nonlinear photon-drag currents purely **q**-odd.

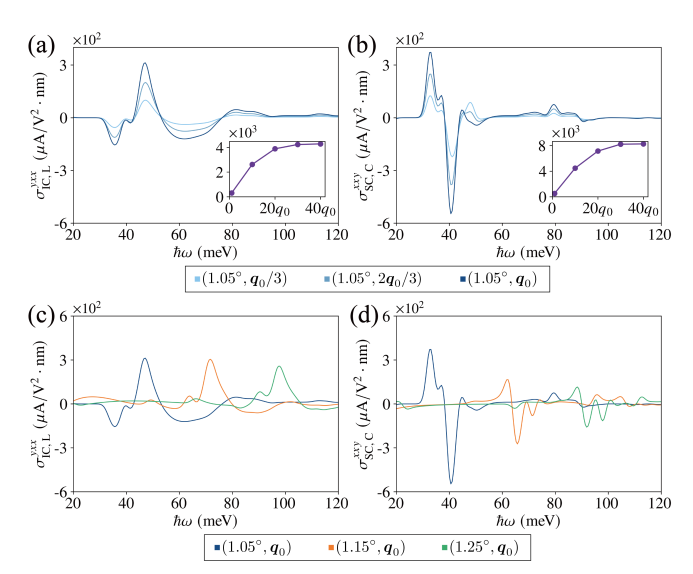


FIG. 2. Photon-drag photoconductivity of centrosymmetric TBG. (a)  $\sigma^{yxx}_{\text{IC,L}}$  and (b)  $\sigma^{xxy}_{\text{SC,C}}$  spectra at  $\theta=1.05^{\circ}$ , showing the evolution with photon wavevector; curves from light to dark correspond to  $q_0/3, 2q_0/3, q_0$ . Insets: magnitude of peak photoconductivity versus  $\boldsymbol{q}$  over an extended range, taken at the spectral peaks  $\hbar\omega=47\text{meV}$  for (a) and  $\hbar\omega=41\text{meV}$  for (b). For (a), we use a moderate relaxation time  $\tau=10^{-13}\,\mathrm{s}$ . (c-d) Spectra at fixed  $\boldsymbol{q}=q_0$  for twist angles  $\theta=1.05^{\circ}, 1.15^{\circ},$  and  $1.25^{\circ}$ , respectively.

Next, we present the numerical results based on the exact continuum model. Unless otherwise specified, we fix the photon wavevector at  $\mathbf{q}_0 = (0, q_0)$  with  $q_0 = 10^{-4} \text{/Å}$ for all photon-drag calculations. Tensor components with an odd number of x indices are omitted, as they are strongly suppressed by the approximate mirror symmetry  $\mathcal{M}_x$  at small twist angles. Figs. 2(a,b) show the spectra at  $\theta = 1.05^{\circ}$  as  $\mathbf{q}$  is varied from  $\mathbf{q}_0/3$  to  $2\mathbf{q}_0/3$ and  $q_0$ . In this small-q window, the peak magnitudes of  $\sigma^{yxx}_{\rm IC,L}(\boldsymbol{q}_{\rm odd})$  and  $\sigma^{xxy}_{\rm SC,C}(\boldsymbol{q}_{\rm odd})$  grow approximately linearly with q, indicating that the response is dominated by the injection- and shift-current dipoles. The insets quantify the scaling over an extended range of q, showing that the peak values increase by nearly an order of magnitude before saturating. Figs. 2(c,d) compare three twist angles  $\theta = 1.05^{\circ}, 1.15^{\circ}, 1.25^{\circ};$  the dominant peaks shift to higher photon energies as  $\theta$  increases, consistent with bandwidth

broadening [31]. To gauge the absolute scale, we take the pronounced peak in  $\sigma^{xxy}_{\rm SC,C}(q_{\rm odd})$  near  $\hbar\omega\simeq41$  meV at  $\theta=1.05^{\circ}$  as a reference. A free-space photon at this energy has wavevector  $q=\omega/c\approx2.03\times10^{-5}/\text{Å}$ ; thus a modest in-plane wavevector only about five times larger already yields sizable nonlinear photocurrents, an order of magnitude larger than the response predicted for the prototypical ferroelectric GeS monolayer [4] and comparable to the giant response predicted for magnetic axion insulators MnBi<sub>2</sub>Te<sub>4</sub> bilayers [5, 32, 33].

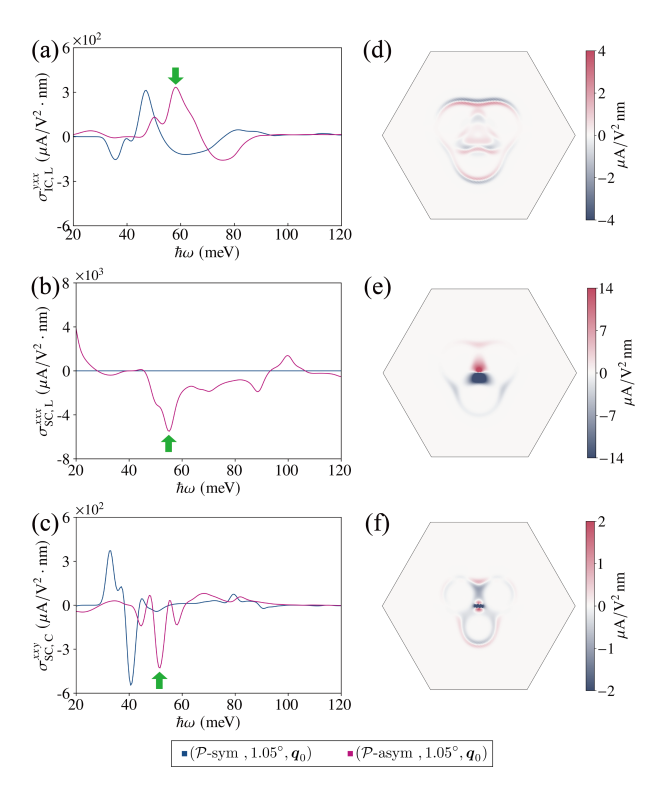


FIG. 3. Influence of inversion symmetry breaking on photon-drag photoconductivity in TBG. (a-c) Photoconductivity spectra in noncentrosymmetric TBG, compared with the centrosymmetric case at  $\theta=1.05^\circ$ : (b)  $\sigma_{\rm IC,L}^{yxx}$ , (c)  $\sigma_{\rm SC,L}^{xxx}$ , (d)  $\sigma_{\rm SC,C}^{xxy}$ . (d-f) k-resolved photoconductivity corresponding to (a-c) at the photon energies indicated by the green arrows in (a-c): (d)  $\hbar\omega=58$  meV, (e)  $\hbar\omega=55$  meV, and (f)  $\hbar\omega=51$  meV.

To extend the analysis to noncentrosymmetric case, we evaluate the effect of a BN-like substrate on the photon-drag response of TBG. We model inversion breaking with a sublattice-staggered potential  $\pm \delta_S$ , taking  $\delta_S = 0.02$  eV on both layers for simplicity [34]. This mimics nearly aligned hBN encapsulation and reduces the point-group symmetry from  $D_{3d}$  to  $D_{3h}$ . Under  $D_{3h}$ ,  $\sigma^{abc}_{\rm IC,C}(\mathbf{q}_{\rm even})$ , which is antisymmetric under index exchange  $b \leftrightarrow c$ , is forbidden. Consequently, the only symmetry-allowed  $\mathbf{q}$ -even contribution is  $\sigma^{abc}_{\rm SC,L}(\mathbf{q}_{\rm even})$ . Within  $\sigma^{abc}_{\rm SC,L}(\mathbf{q}_{\rm even})$ , only components with an even number of y indices (e.g., xxx, xyy) remain sizable, because the shift-current quadrupole is negligible in the small-q regime and the approximate mirror  $\mathcal{M}_y$  strongly suppresses odd-y terms.

Consistent with the symmetry analysis,  $\sigma_{\text{SCLL}}^{xxx}(q_{\text{even}})$  is negligable in the  $\mathcal{P}$ -symmetric case and becomes significant once  $\delta_S \neq 0$ , as depicted in Fig. 3(b). The **q**odd responses, namely  $\sigma^{yxx}_{\rm IC,L}(\boldsymbol{q}_{\rm odd})$  and  $\sigma^{xxy}_{\rm SC,C}(\boldsymbol{q}_{\rm odd})$ , remain allowed irrespective of  $\mathcal P$  and exhibit modest lineshape shifts that track the inversion-breaking-induced gap opening, as shown in Figs. 3(a,c) [35]. Comparing Fig. 3(b) with Figs. 3(a,c), we observe that the linear shift current exceeds the linear injection and circular shift currents by roughly an order of magnitude, which reflects the small-q scaling. However, once q saturates, the qodd response is expected to become comparable to the q-even response. To clarify the microscopic origin of the signals, we evaluate the k-resolved photoconductivity at representative spectral peaks. From Figs.3(d-f), the finite response is dominated by interband transitions near the  $\Gamma$  point, specifically from the flat valence band to the dispersive conduction band. In k space, the textures of  $\sigma^{yxx}_{\text{IC,L}}(\boldsymbol{q}_{\text{odd}})$  and  $\sigma^{xxy}_{\text{SC,C}}(\boldsymbol{q}_{\text{odd}})$  display alternating positivenegative lobes arranged in closely spaced stripes, whereas  $\sigma^{xxx}_{ ext{SC,L}}(m{q}_{ ext{even}})$  does not exhibit this feature. This contrast follows from the former two being governed by injectionand shift-current dipoles, while the latter arises from the shift current.

Conclusion.—We have developed a geometric-loop formalism that unifies the photon-drag injection and shift current contributions within a single, transparent framework, providing clear quantum-geometric insight while remaining numerically efficient. Using this approach, we derive general symmetry constraints on the nonlinear photon-drag conductivity tensor, identifying the symmetry allowed components under  $\mathcal{P}$ ,  $\mathcal{T}$ , and their combinations. Applied to the TBG through a realistic continuum model incorporating atomic relaxation and particlehole asymmetry, the formalism reveals that even modest in-plane photon wavevectors can induce sizable nonlinear currents in centrosymmetric TBG. Near twist angles slightly above the magic value ( $\sim 1.05^{\circ}$ ), the predicted photon-drag injection and shift currents reach magnitudes comparable to the giant conventional photogalvanic response reported in typical noncentrosymmetric two-dimensional materials. The dependence on photon momentum is approximately linear in the smallq regime, a clear signature of the injection- and shiftcurrent dipoles mechanisms. As photon wavevector increases, the peak response grows by nearly an order of magnitude before eventually saturating. We traced the evolution of the photon-drag spectra with twist angle, finding that the peak shifts to higher photon energy as the bandwidth broadens with increasing twist angle. For TBG aligned with hBN, inversion breaking enables a conventional shift current that dominates at small at small q and exceeds the leading  $q^1$  contributions by roughly an order of magnitude. The momentum-space distribution of the shift current differs qualitatively from that of the photon-drag contributions, underscoring the distinct physical mechanisms. Overall, these results demonstrate that exploiting light's momentum enables large nonlinear

dc photocurrents in moiré systems such as TBG, opening avenues for photon-drag-engineered optoelectronic functionalities

Acknowledgements.—H.W. acknowledges the support from the NSFC under Grants Nos. 12522411, 12474240,

and 12304049, as well as the support from Fundamental Research Funds for the Central Universities. K. C. acknowledges the support from the NSFC under Grants No. 12488101, and the Innovation Program for Quantum Science and Technology under Grant No. 2024ZD0300104.

- P. Hosur, Circular photogalvanic effect on topological insulator surfaces: Berry-curvature-dependent response, Phys. Rev. B 83, 035309 (2011).
- [2] T. Morimoto and N. Nagaosa, Topological nature of nonlinear optical effects in solids, Sci. Adv. 2, e1501524 (2016).
- [3] F. de Juan, A. G. Grushin, T. Morimoto, and J. E. Moore, Quantized circular photogalvanic effect in weyl semimetals, Nat. Commun. 8, 15995 (2017).
- [4] T. Rangel, B. M. Fregoso, B. S. Mendoza, T. Morimoto, J. E. Moore, and J. B. Neaton, Large bulk photovoltaic effect and spontaneous polarization of single-layer monochalcogenides, Phys. Rev. Lett. 119, 067402 (2017).
- [5] H. Wang and X. Qian, Electrically and magnetically switchable nonlinear photocurrent in pt-symmetric magnetic topological quantum materials, npj Comput. Mater. 6, 199 (2020).
- [6] J. Ahn, G.-Y. Guo, and N. Nagaosa, Low-frequency divergence and quantum geometry of the bulk photovoltaic effect in topological semimetals, Phys. Rev. X 10, 041041 (2020).
- [7] J. Ahn, G.-Y. Guo, N. Nagaosa, and A. Vishwanath, Riemannian geometry of resonant optical responses, Nat. Phys. 18, 290 (2022).
- [8] S. Chaudhary, C. Lewandowski, and G. Refael, Shiftcurrent response as a probe of quantum geometry and electron-electron interactions in twisted bilayer graphene, Phys. Rev. Research 4, 013164 (2022).
- [9] R. Resta, Geometrical theory of the shift current in presence of disorder and interaction, Phys. Rev. Lett. 133, 206903 (2024).
- [10] J. Sivianes, F. J. D. Santos, and J. Ibañez-Azpiroz, Optical signatures of spin symmetries in unconventional magnets, Phys. Rev. Lett. 134, 196907 (2025).
- [11] A. Avdoshkin, J. Mitscherling, and J. E. Moore, Multistate geometry of shift current and polarization, Phys. Rev. Lett. 135, 066901 (2025).
- [12] Z. Ji, G. Liu, Z. Addison, W. Liu, P. Yu, H. Gao, Z. Liu, A. M. Rappe, C. L. Kane, E. J. Mele, and R. Agarwal, Spatially dispersive circular photogalvanic effect in a weyl semimetal, Nat. Mater. 18, 955 (2019).
- [13] H. J. Lezec, A. Degiron, E. Devaux, R. A. Linke, L. Martin-Moreno, F. J. Garcia-Vidal, and T. W. Ebbesen, Beaming light from a subwavelength aperture, Science 297, 820 (2002).
- [14] D. N. Basov, M. M. Fogler, and F. J. García De Abajo, Polaritons in van der waals materials, Science 354, aag1992 (2016).
- [15] Y. Kurman, N. Rivera, T. Christensen, S. Tsesses, M. Orenstein, M. Soljačić, J. D. Joannopoulos, and I. Kaminer, Control of semiconductor emitter frequency by increasing polariton momenta, Nature Photon 12, 423 (2018).
- [16] L.-k. Shi, D. Zhang, K. Chang, and J. C. W. Song, Geo-

- metric photon-drag effect and nonlinear shift current in centrosymmetric crystals, Phys. Rev. Lett. **126**, 197402 (2021).
- [17] Y.-M. Xie and N. Nagaosa, Photon-drag photovoltaic effects and quantum geometric nature, Proc. Natl. Acad. Sci. U.S.A. 122, e2424294122 (2025).
- [18] Y. Cao, V. Fatemi, A. Demir, S. Fang, S. L. Tomarken, J. Y. Luo, J. D. Sanchez-Yamagishi, K. Watanabe, T. Taniguchi, E. Kaxiras, R. C. Ashoori, and P. Jarillo-Herrero, Correlated insulator behaviour at half-filling in magic-angle graphene superlattices, Nature 556, 80 (2018).
- [19] Y. Cao, V. Fatemi, S. Fang, K. Watanabe, T. Taniguchi, E. Kaxiras, and P. Jarillo-Herrero, Unconventional superconductivity in magic-angle graphene superlattices, Nature 556, 43 (2018).
- [20] X. Lu, P. Stepanov, W. Yang, M. Xie, M. A. Aamir, I. Das, C. Urgell, K. Watanabe, T. Taniguchi, G. Zhang, A. Bachtold, A. H. MacDonald, and D. K. Efetov, Superconductors, orbital magnets and correlated states in magic-angle bilayer graphene, Nature 574, 653 (2019).
- [21] M. Serlin, C. L. Tschirhart, H. Polshyn, Y. Zhang, J. Zhu, K. Watanabe, T. Taniguchi, L. Balents, and A. F. Young, Intrinsic quantized anomalous hall effect in a moiré heterostructure, Science 367, 900 (2020).
- [22] Y. Xie, A. T. Pierce, J. M. Park, D. E. Parker, E. Khalaf, P. Ledwith, Y. Cao, S. H. Lee, S. Chen, P. R. Forrester, K. Watanabe, T. Taniguchi, A. Vishwanath, P. Jarillo-Herrero, and A. Yacoby, Fractional chern insulators in magic-angle twisted bilayer graphene, Nature 600, 439 (2021).
- [23] P. Stepanov, M. Xie, T. Taniguchi, K. Watanabe, X. Lu, A. H. MacDonald, B. A. Bernevig, and D. K. Efetov, Competing zero-field chern insulators in superconducting twisted bilayer graphene, Phys. Rev. Lett. 127, 197701 (2021).
- [24] Y.-H. Zhang, D. Mao, and T. Senthil, Twisted bilayer graphene aligned with hexagonal boron nitride: Anomalous hall effect and a lattice model, Phys. Rev. Res. 1, 033126 (2019).
- [25] A. Abouelkomsan, Z. Liu, and E. J. Bergholtz, Particle-hole duality, emergent fermi liquids, and fractional chern insulators in moiré flatbands, Phys. Rev. Lett. 124, 106803 (2020).
- [26] See Sec. A, Sec. B and Sec. C of the Supplemental Material for a detailed derivation of nonlinear photon-drag photoconductivity.
- [27] See Sec. D of the Supplemental Material for a detailed derivation of geometric-loop formalism.
- [28] See Sec. E of the Supplemental Material for a detailed symmetry analysis of nonlinear photon-drag photoconductivity.
- [29] S. Carr, S. Fang, Z. Zhu, and E. Kaxiras, Exact continuum model for low-energy electronic states of twisted

- bilayer graphene, Phys. Rev. Research 1, 013001 (2019).
- [30] R. Bistritzer and A. H. MacDonald, Moiré bands in twisted double-layer graphene, Proc. Natl. Acad. Sci. U.S.A. 108, 12233 (2011).
- [31] Band structures for three different twist angles are provided in the Supplemental Material, Sec. F.
- [32] R. Fei, W. Song, and L. Yang, Giant photogalvanic effect and second-harmonic generation in magnetic axion insulators, Phys. Rev. B 102, 035440 (2020).
- [33] H. Xu, H. Wang, J. Zhou, and J. Li, Pure spin photocurrent in non-centrosymmetric crystals: Bulk spin photovoltaic effect, Nat Commun 12, 4330 (2021).
- [34] S. Carr, S. Fang, H. C. Po, A. Vishwanath, and E. Kaxiras, Derivation of wannier orbitals and minimal-basis tight-binding hamiltonians for twisted bilayer graphene: First-principles approach, Phys. Rev. Research 1, 033072 (2019).
- [35] Band structures for centrosymmetric and noncentrosymmetric TBG are provided in the Supplemental Material, Sec. F.
- [36] H. Wang, X. Tang, H. Xu, J. Li, and X. Qian, Generalized wilson loop method for nonlinear light-matter interaction, npj Quantum Mater. 7, 61 (2022).

#### Supplementary Material

- A. Density matrix theory for inhomogeous optical electric field 7
- B. Photon-drag injection current
- C. Photon-drag shift current
- D. Geometric-loop formalism for photon-drag shift current photoconductivity 11
- E. Symmetry analysis for nonlinear photon-drag photoconductivity 12
- F. Continuum-model band structures of twisted bilayer graphene 13

#### A. Density matrix theory for inhomogeous optical electric field

For system illuminated by inhomogeous optical electric field, the Hamiltonian can be expressed as

$$\hat{H} = \hat{H}^{(0)} + \hat{H}^{(1)} + \hat{H}_{s} \tag{A1}$$

where  $\hat{H}^{(0)}$  is the unperturbed Hamiltonian,

$$\hat{H}^{(1)} = -\frac{e}{2} \left( \boldsymbol{A}(\boldsymbol{r}, t) \cdot \hat{\boldsymbol{v}}^{(0)} + \hat{\boldsymbol{v}}^{(0)} \cdot \boldsymbol{A}(\boldsymbol{r}, t) \right)$$
(A2)

indicates the coupling between the optical field and the system,  $\hat{H}_s$  describes the scattering effects. Here, e = -|e|,  $\hat{v}^{(0)}$  is the velocity operator of  $\hat{H}^{(0)}$ ,  $\mathbf{A}(\mathbf{r},t) = \mathbf{A}(\omega)e^{i\mathbf{q}\cdot\mathbf{r}-i\omega t} + \mathbf{A}(-\omega)e^{-i\mathbf{q}\cdot\mathbf{r}+i\omega t}$  is the inhomogeous vector field.

To access the density corrections induced by optical electric field, we need to solve the quantum Liouville equation

$$i\hbar \frac{d\rho}{dt} = [\hat{H}, \rho] \tag{A3}$$

in Bloch representation. Inserting Eq. (A1) into Eq. (A3) and consider the matrix element between Bloch states  $\langle u_{\alpha}|...|u_{\beta}\rangle$ , we have

$$\frac{d\rho_{\alpha\beta}}{dt} = -i\omega_{\alpha\beta}\rho_{\alpha\beta} - \frac{e}{\hbar\omega}E_b(\omega)e^{-i\omega t}\sum_{n_{\gamma}} \left(v_{\alpha\gamma}^b\rho_{\gamma\beta} - \rho_{\alpha\gamma}v_{\gamma\beta}^b\right) - \frac{\rho_{\alpha\beta} - \rho_{\alpha\beta}^{(0)}}{\tau},\tag{A4}$$

where  $\alpha=(n_{\alpha}, \boldsymbol{k}_{\alpha}), \ \beta=(n_{\beta}, \boldsymbol{k}_{\beta})$  and  $\gamma=(n_{\gamma}, \boldsymbol{k}_{\gamma})$  are composite index for band and wavevector, velocity matrix element is defined as  $v_{\alpha\beta}^b=\langle u_{\alpha}|\hat{v}_{\alpha,\beta}^b|u_{\beta}\rangle, \ \hat{v}_{\alpha,\beta}^b\equiv\frac{1}{2}(\hat{v}_{\boldsymbol{k}_{\alpha}}^b+\hat{v}_{\boldsymbol{k}_{\beta}}^b)$ , we have  $\boldsymbol{k}_{\alpha}-\boldsymbol{k}_{\gamma}=\boldsymbol{q}$  for  $v_{\alpha\gamma}^b$  and  $\boldsymbol{k}_{\gamma}-\boldsymbol{k}_{\beta}=\boldsymbol{q}$  for  $v_{\gamma\beta}^b$ . Generally,  $\boldsymbol{k}_{\gamma}$  in the first and second terms are different. In the right hand side of Eq. (A4), the first term comes from the commutator  $[\hat{H}^{(0)},\rho]$ , the second term comes from the commutator  $[\hat{H}^{(1)},\rho]$  and the third term comes from the commutator  $[\hat{H}_s,\rho]$  and treated with relaxation time approximation,  $\tau$  is the phenomenlogical relaxation time. For brevity, summation over Cartesian index b is implicit and contribution from  $(\boldsymbol{q},\omega)\to(-\boldsymbol{q},-\omega)$  will be restored in the end of the derivation.

The density matrix  $\rho_{\alpha\beta}$  can be expanded according to the order of optical electric field as

$$\rho_{\alpha\beta} = \rho_{\alpha\beta}^{(0)} + \rho_{\alpha\beta}^{(1)} + \rho_{\alpha\beta}^{(2)} + \dots$$
 (A5)

Insert Eq. (A5) into Eq. (A4), we can iteratively solve the density matrix of each order. Inserting zeroth order density matrix  $\rho_{\alpha\beta}^{(0)} = \delta_{\alpha\beta} f_{\alpha}$  into the Eq. (A4) and keeping only the terms that are linear in optical electric field, we can access the first-order density matrix  $\rho_{\alpha\beta}^{(1)}$  as

$$\rho_{\alpha\beta}^{(1)} = \frac{e}{i\hbar\omega} E_b(\omega) e^{-i\omega t} \frac{f_{\alpha\beta} v_{\alpha\beta}^b}{\omega_{\alpha\beta} - \omega - i\tau^{-1}},\tag{A6}$$

where  $f_{\alpha\beta} = f_{\alpha} - f_{\beta}$  is the difference of occupation,  $\mathbf{k}_{\alpha} = \mathbf{k} + \mathbf{q}/2$  and  $\mathbf{k}_{\beta} = \mathbf{k} - \mathbf{q}/2$ .

Furthermore, inserting first-order density matrix  $\rho_{\alpha\beta}^{(1)}$  into Eq. (A6) and keeping only the terms that are second-order in optical electric field, we can access the second-order density matrix as

$$\rho_{\alpha\beta}^{(2)} = E_b(\omega)E_c(-\omega)\frac{-e^2}{\hbar^2\omega^2}\sum_{n_\gamma}\frac{v_{\alpha\gamma}^c v_{\gamma\beta}^b}{\omega_{\alpha\beta} - i\tau^{-1}} \left(\frac{f_{\gamma\beta}}{\omega_{\gamma\beta} - \omega - i\tau^{-1}} - \frac{f_{\alpha\gamma}}{\omega_{\alpha\gamma} + \omega - i\tau^{-1}}\right),\tag{A7}$$

where  $\mathbf{k}_{\alpha} = \mathbf{k}_{\beta} = \mathbf{k} - \mathbf{q}/2$  and  $\mathbf{k}_{\gamma} = \mathbf{k} + \mathbf{q}/2$ .

For the Hamiltonian given in Eq. (A1), current operator  $\hat{j} = e\hat{v}$  explicitly depends on the external field. Thus the expectation value of second-order photocurrent constitute of two part:

$$\boldsymbol{J}^{(2)} = e \int [d\boldsymbol{k}] \sum_{n_{\alpha}, n_{\beta}} \boldsymbol{v}_{\beta\alpha}^{(0)} \rho_{\alpha\beta}^{(2)} + \boldsymbol{v}_{\beta\alpha}^{(1)} \rho_{\alpha\beta}^{(1)}, \tag{A8}$$

where  $\int [d\mathbf{k}] \equiv \int d^d\mathbf{k}/(2\pi)^d$ . Here, the first term involves the matrix elements of the zeroth-order velocity operator  $v^{(0)}$  weighted by the second-order density matrix  $\rho^{(2)}$ , whereas the second term combines the first-order velocity operator  $v^{(1)}$  with the first-order density matrix  $\rho^{(1)}$ .

# B. Photon-drag injection current

In this section, we derive the photon-drag injection current from the diagonal component of the density matrix in Eq. (A8), i.e.

$$\mathbf{J}_{\rm IC} = e \int [d\mathbf{k}] \sum_{n_{\alpha}} \mathbf{v}_{\alpha\alpha}^{(0)} \rho_{\alpha\alpha}^{(2)}. \tag{B1}$$

Note that  $\rho_{\alpha\alpha}^{(1)}$  contains no resonant terms and is therefore neglected.

The diagonal part of the second-order density matrix  $\rho_{\alpha\alpha}^{(2)}$  takes the form

$$\rho_{\alpha\alpha}^{(2)} = E_b(\omega)E_c(-\omega)\frac{-2\tau\pi e^2}{\hbar^2\omega^2}\sum_{n_\beta}f_{\alpha\beta}\delta(\omega_{\beta\alpha} - \omega)v_{\alpha\beta}^c v_{\beta\alpha}^b,$$
(B2)

where  $\mathbf{k}_{\alpha} = \mathbf{k} - \mathbf{q}/2$  and  $\mathbf{k}_{\beta} = \mathbf{k} + \mathbf{q}/2$ . We have used the identity  $\{x - i\eta\}^{-1} \approx P\{x^{-1}\} + i\pi\delta(x)$ , with  $P\{...\}$  denoting the principal part. Substituting Eq. (B2) into Eq. (B1) yields

$$J_{\rm IC}^a = \sigma_{\rm IC}^{abc}(\boldsymbol{q}, \omega) E_b(\omega) E_c(-\omega), \tag{B3}$$

with

$$\sigma_{\rm IC}^{abc}(\boldsymbol{q},\omega) = \frac{-2\tau\pi e^3}{\hbar^2\omega^2} \int [d\boldsymbol{k}] \sum_{n_\alpha,n_\beta} f_{\alpha\beta} \delta(\omega_{\beta\alpha} - \omega) v_{\beta\alpha}^b v_{\alpha\beta}^c v_{\alpha\alpha}^a, \tag{B4}$$

Including the contribution from  $(q, \omega) \to (-q, -\omega)$  via  $\alpha \leftrightarrow \beta$  and  $b \leftrightarrow c$ , we obtain

$$\sigma_{\rm IC}^{abc}(\boldsymbol{q},\omega) = \frac{2\tau\pi e^3}{\hbar^2\omega^2} \int [d\boldsymbol{k}] \sum_{n_{\alpha},n_{\beta}} f_{\alpha\beta} \delta(\omega_{\beta\alpha} - \omega) v_{\beta\alpha}^b v_{\alpha\beta}^c \left(v_{\beta\beta}^a - v_{\alpha\alpha}^a\right). \tag{B5}$$

Eq. (B5) shows that  $\sigma_{\rm IC}^{abc}$  scales with the relaxation time and the velocity difference between conduction and valence bands, in agreement with the standard injection mechanism in homogeneous density matrix theory. As a consistency check, taking the homogeneous limit  $q \to 0$  recovers the usual injection current photoconductivity:

$$\sigma_{\rm IC}^{abc}(\omega) = \frac{2\tau\pi e^3}{\hbar^2} \int [d\mathbf{k}] \sum_{n,m} f_{nm} \delta(\omega_{mn} - \omega) r_{mn}^b r_{nm}^c \left(v_{mm}^a - v_{nn}^a\right),\tag{B6}$$

where we have moved the factor  $\omega^{-2}$  inside the integral as  $\omega_{mn}^{-2}$  and used  $v_{nm}^a = i\omega_{nm}r_{nm}^a$ , with  $r_{nm}^a$  denoting the interband Berry connection.

# C. Photon-drag shift current

We now demonstrate that the photon-drag shift current stems from the off-diagonal components of the density matrix in Eq. (A8), namely:

$$\boldsymbol{J}_{SC} = \boldsymbol{J}_{od\text{-}2nd} + \boldsymbol{J}_{od\text{-}1st} = e \int [d\boldsymbol{k}] \sum_{n_{\alpha}, n_{\beta} \neq n_{\alpha}} \boldsymbol{v}_{\beta\alpha}^{(0)} \rho_{\alpha\beta}^{(2)} + \boldsymbol{v}_{\beta\alpha}^{(1)} \rho_{\alpha\beta}^{(1)}.$$
(C1)

We first consider  $J_{\text{od-2nd}}$ , which reads

$$J_{\text{od-2nd}}^{a} = \sigma_{\text{2nd-od}}^{abc}(\boldsymbol{q}, \omega) E_{b}(\omega) E_{c}(-\omega), \tag{C2}$$

with

$$\sigma_{\text{od-2nd}}^{abc}(\boldsymbol{q},\omega) = \frac{-\pi e^3}{\hbar^2 \omega^2} \int [d\boldsymbol{k}] \sum_{n_{\alpha},n_{\beta} \neq n_{\alpha},n_{\gamma}} r_{\beta\alpha}^a v_{\alpha\gamma}^c v_{\gamma\beta}^b (f_{\gamma\beta}\delta(\omega_{\gamma\beta} - \omega) - f_{\alpha\gamma}\delta(\omega_{\alpha\gamma} + \omega)), \tag{C3}$$

where  $\mathbf{k}_{\alpha} = \mathbf{k}_{\beta} = \mathbf{k} - \mathbf{q}/2$  and  $\mathbf{k}_{\gamma} = \mathbf{k} + \mathbf{q}/2$ . Here we retain only the resonant  $\delta$ -function terms. Using identities

$$\sum_{n_{\alpha} \neq n_{\beta}} r_{\beta\alpha}^{a} v_{\alpha\gamma}^{c} = -i \langle \partial_{k^{a}} u_{\beta} | \hat{v}_{\beta,\gamma}^{c} | u_{\gamma} \rangle - r_{\beta\beta}^{a} v_{\beta\gamma}^{c}$$

$$\sum_{n_{\beta} \neq n_{\alpha}} v_{\gamma\beta}^{b} r_{\beta\alpha}^{a} = i \langle u_{\gamma} | \hat{v}_{\gamma,\alpha}^{b} | \partial_{k^{a}} u_{\alpha} \rangle - v_{\gamma\alpha}^{b} r_{\alpha\alpha}^{a},$$
(C4)

we recast Eq. (C3) as

$$\sigma_{\text{od-2nd}}^{abc}(\boldsymbol{q},\omega) = \frac{i\pi e^3}{\hbar^2 \omega^2} \int_{\boldsymbol{k}} \sum_{n_a,n_\beta} f_{\alpha\beta} \delta(\omega_{\beta\alpha} - \omega) \left( -\langle \partial_{k^a} u_\alpha | \hat{v}_{\alpha,\beta}^c | u_\beta \rangle v_{\beta\alpha}^b + v_{\alpha\beta}^c \langle u_\beta | \hat{v}_{\beta,\alpha}^b | \partial_{k^a} u_\alpha \rangle + 2ir_{\alpha\alpha}^a v_{\alpha\beta}^c v_{\beta\alpha}^b \right), \quad (C5)$$

where  $\mathbf{k}_{\alpha} = \mathbf{k} - \mathbf{q}/2$  and  $\mathbf{k}_{\beta} = \mathbf{k} + \mathbf{q}/2$ .

Including the contribution from  $(\mathbf{q}, \omega) \to (-\mathbf{q}, -\omega)$  via  $\alpha \leftrightarrow \beta$  and  $b \leftrightarrow c$  gives

$$\sigma_{\text{od-2nd}}^{abc}(\boldsymbol{q},\omega) = \frac{i\pi e^3}{\hbar^2 \omega^2} \int [d\boldsymbol{k}] \sum_{n_{\alpha},n_{\beta}} f_{\alpha\beta} \delta(\omega_{\beta\alpha} - \omega) \left[ \left( v_{\beta\alpha}^{b;a} v_{\alpha\beta}^c - v_{\beta\alpha}^b v_{\alpha\beta}^{c;a} \right) + \left( v_{\beta\alpha}^b w_{\alpha\beta}^{ca} - w_{\beta\alpha}^{ba} v_{\alpha\beta}^c \right) \right], \tag{C6}$$

where  $v_{\beta\alpha}^{b;a} = \partial_{k^a} v_{\beta\alpha}^b - i(r_{\beta\beta}^a - r_{\alpha\alpha}^a)v_{\beta\alpha}^b$  is the generalized derivative and  $w_{\alpha\beta}^{ca} = \langle u_\alpha | \partial_{k^a} \hat{v}_{\alpha,\beta}^c | u_\beta \rangle$  the inverse effective mass matrix.

Next, we express the first-order velocity matrix

$$\hat{v}^{a,(1)} = \frac{1}{i\hbar} \left[ \hat{r}^a, \hat{H}^{(1)} \right] \tag{C7}$$

in Bloch representation, which yields

$$\langle \psi_{\beta} | \hat{v}^{a,(1)} | \psi_{\alpha} \rangle = E_b(\omega) e^{-i\omega t} \frac{-ie}{\hbar \omega} w_{\beta\alpha}^{ba}, \tag{C8}$$

where  $\mathbf{k}_{\alpha} = \mathbf{k} - \mathbf{q}/2$  and  $\mathbf{k}_{\beta} = \mathbf{k} + \mathbf{q}/2$ . Using the  $(-\mathbf{q}, -\omega)$  counterpart of  $\rho_{\alpha\beta}^{(1)}$  and retain the resonant part, we obtain

$$J_{\text{od-1st}}^{a} = \sigma_{\text{od-1st}}^{abc}(\boldsymbol{q}, \omega) E_{b}(\omega) E_{c}(-\omega), \tag{C9}$$

with

$$\sigma_{\text{1st-od}}^{abc}(\boldsymbol{q},\omega) = \frac{i\pi e^3}{\hbar^2 \omega^2} \int [d\boldsymbol{k}] \sum_{n_{\alpha},n_{\beta}} f_{\alpha\beta} \delta(\omega_{\beta\alpha} - \omega) w_{\beta\alpha}^{ba} v_{\alpha\beta}^c, \tag{C10}$$

where

$$\rho_{\alpha\beta}^{(1)} = \frac{-\pi e}{\hbar \omega} E_c(-\omega) e^{i\omega t} f_{\alpha\beta} \delta(\omega_{\beta\alpha} - \omega) v_{\alpha\beta}^c. \tag{C11}$$

Including the contribution from  $(q, \omega) \to (-q, -\omega)$  via  $\alpha \leftrightarrow \beta$  and  $b \leftrightarrow c$  gives

$$\sigma_{\text{od-1st}}^{abc}(\boldsymbol{q},\omega) = \frac{-i\pi e^3}{\hbar^2 \omega^2} \int [d\boldsymbol{k}] \sum_{n_{\alpha},n_{\beta}} f_{\alpha\beta} \delta(\omega_{\beta\alpha} - \omega) \left( v_{\beta\alpha}^b w_{\alpha\beta}^{ca} - w_{\beta\alpha}^{ba} v_{\alpha\beta}^c \right). \tag{C12}$$

Thus, we obtain:

$$J_{\rm SC}^a = \sigma_{\rm SC}^{abc}(\mathbf{q}, \omega) E_b(\omega) E_c(-\omega), \tag{C13}$$

with

$$\sigma_{\rm SC}^{abc}(\boldsymbol{q},\omega) = \frac{i\pi e^3}{\hbar^2 \omega^2} \int [d\boldsymbol{k}] \sum_{n_{\alpha},n_{\beta}} f_{\alpha\beta} \delta(\omega_{\beta\alpha} - \omega) \left( v_{\beta\alpha}^{b;a} v_{\alpha\beta}^{c} - v_{\beta\alpha}^{b} v_{\alpha\beta}^{c;a} \right), \tag{C14}$$

where  $\mathbf{k}_{\alpha} = \mathbf{k} - \mathbf{q}/2$  and  $\mathbf{k}_{\beta} = \mathbf{k} + \mathbf{q}/2$ . Comparing Eq. (C14) with Eq. (C3) and Eq. (C12), we find  $v_{\beta\alpha}^{b;a}$  satisfies the following sum rule

$$v_{\beta\alpha}^{b;a} = w_{\beta\alpha}^{ba} - \sum_{n_{\gamma} \neq n_{\beta}} \frac{v_{\beta\gamma}^{a} v_{\gamma\alpha}^{b}}{\omega_{\gamma\beta}} + \sum_{n_{\gamma} \neq n_{\alpha}} \frac{v_{\beta\gamma}^{b} v_{\gamma\alpha}^{a}}{\omega_{\alpha\gamma}}, \tag{C15}$$

where  $k_{\gamma} = k + q/2$  for the summation  $\sum_{n_{\gamma} \neq n_{\beta}}$  and  $k_{\gamma} = k - q/2$  for the summation  $\sum_{n_{\gamma} \neq n_{\alpha}}$ . We can also express  $\sigma_{\rm SC}^{abc}$  as:

$$\sigma_{\rm SC}^{abc}(\boldsymbol{q},\omega) = \frac{\pi e^3}{\hbar^2 \omega^2} \int [d\boldsymbol{k}] \sum_{n_\alpha,n_\beta} f_{\alpha\beta} \delta(\omega_{\beta\alpha} - \omega) v_{\beta\alpha}^b v_{\alpha\beta}^c \left( R_{\beta\alpha}^{b;a} - R_{\alpha\beta}^{c;a} \right), \tag{C16}$$

realizing that  $v_{\beta\alpha}^{b;a} = -iR_{\beta\alpha}^{b;a}v_{\beta\alpha}^{b}$  with

$$R_{\beta\alpha}^{b;a} = i\partial_{ka}\log v_{\beta\alpha}^b + r_{\beta\beta}^b - r_{\alpha\alpha}^b \tag{C17}$$

is the well-known shift vector extended to the case with nonzero momentum transfer. As  $q \to 0$ , Eq. (C16) reduces to the conventional shift-current photoconductivity:

$$\sigma_{\rm SC}^{abc}(\omega) = \frac{\pi e^3}{\hbar^2} \int [d\mathbf{k}] \sum_{n,m} f_{nm} \delta(\omega_{mn} - \omega) r_{mn}^b r_{nm}^c \left( R_{mn}^{b;a} - R_{nm}^{c;a} \right), \tag{C18}$$

if noting that

$$i\partial_{k_{a}} \log v_{mn}^{b} + r_{mm}^{a} - r_{nn}^{a} = R_{mn}^{b;a} + \frac{i(v_{mm}^{a} - v_{nn}^{a})}{\omega_{mn}}$$

$$i\partial_{k_{a}} \log v_{nm}^{c} + r_{nn}^{a} - r_{mm}^{a} = R_{nm}^{c;a} + \frac{i(v_{mm}^{a} - v_{nn}^{a})}{\omega_{mn}}.$$
(C19)

Here,  $R_{mn}^{b;a} = i\partial_{k_a} \log r_{mn}^c + r_{mm}^a - r_{nn}^a$  is the conventional shift vector, which involves no momentum transfer. Eq. (C16) has a clear quantum-geometric interpretation: the wavepacket shift between conduction and valence bands  $R_{\beta\alpha}^{b;a}$  weighted by the optical matrix elements  $v_{\alpha\beta}^c v_{\beta\alpha}^b$  and the joint density of states  $f_{\alpha\beta}\delta(\omega_{\beta\alpha}-\omega)$ . Although  $R_{\beta\alpha}^{b;a}$  is gauge-invariant, it is built from the derivative of the gauge-dependent velocity matrix and therefore not directly amenable to numerical evaluation. On the other hand, Eq. (C14), with the sum rule in Eq. (C15), is numerically tractable but obscures the underlying quantum-geometric picture, since it requires summing over multiple terms and different bands. In the next section we derive an alternative form of the photon-drag shift current photoconductivity that retains a direct link to the quantum geometry while remaining efficient for numerical evaluation.

# D. Geometric-loop formalism for photon-drag shift current photoconductivity

For readiblity, we recite the microscopic expression of photon-drag shift current photoconductivity here,

$$\sigma_{\rm SC}^{abc}(\boldsymbol{q},\omega) = \frac{\pi e^3}{\hbar^2 \omega^2} \int [d\boldsymbol{k}] \sum_{n_\alpha,n_\beta} f_{\alpha\beta} \delta(\omega_{\beta\alpha} - \omega) v_{\beta\alpha}^b v_{\alpha\beta}^c \left( R_{\beta\alpha}^{b;a} - R_{\alpha\beta}^{c;a} \right), \tag{D1}$$

in which shift vector is

$$R_{\beta\alpha}^{b;a} = i\partial_{k^a} \log v_{\beta\alpha}^b + r_{\beta\beta}^a - r_{\alpha\alpha}^a, \tag{D2}$$

 $\alpha$  and  $\beta$  are composite index for state before and after photoexcitation with  $\mathbf{k}_{\alpha} = \mathbf{k} - \mathbf{q}/2$ ,  $\mathbf{k}_{\beta} = \mathbf{k} + \mathbf{q}/2$ . Noting that

$$r_{\beta\beta}^{a} = i\partial_{p} \log \langle u_{\beta} | u_{\beta'} \rangle$$

$$r_{\alpha\alpha}^{a} = -i\partial_{p} \log \langle u_{\alpha'} | u_{\alpha} \rangle$$
(D3)

with  $\alpha' = (n_{\alpha}, \mathbf{k}_{\alpha} + p\hat{\mathbf{a}}), \beta' = (n_{\beta}, \mathbf{k}_{\beta} + p\hat{\mathbf{a}})$ , where p is an infinitesimal displacement evaluated in the limit  $p \to 0^+$ , we can then rewrite the shift vector as:

$$R_{\beta\alpha}^{b;a} = i\partial_p \log \langle u_\beta | u_{\beta'} \rangle \langle u_{\beta'} | \hat{v}_{\beta',\alpha'}^b | u_{\alpha'} \rangle \langle u_{\alpha'} | u_{\alpha} \rangle. \tag{D4}$$

Since  $\langle u_{\alpha}|\hat{v}_{\alpha,\beta}^c|u_{\beta}\rangle$  is independent of p, we can further rewrite shift vector as

$$R_{\beta\alpha}^{b;a} = \hat{D}_p \log \mathcal{L}_{\beta\alpha}^{abc} (p) \tag{D5}$$

where we define

$$\mathcal{L}_{\beta\alpha}^{abc}(p) = \langle u_{\beta} | u_{\beta'} \rangle \langle u_{\beta'} | \hat{v}_{\beta',\alpha'}^b | u_{\alpha'} \rangle \langle u_{\alpha'} | u_{\alpha} \rangle \langle u_{\alpha} | \hat{v}_{\alpha,\beta}^c | u_{\beta} \rangle, \tag{D6}$$

and  $\hat{D}_p = i\partial_p$  is the dipole operator. Alternatively,  $\mathcal{L}^{abc}_{\beta\alpha}(p)$  can be recast into a more compact form:

$$\mathcal{L}_{\beta\alpha}^{abc}(p) = \langle P_{\beta'} \hat{v}_{\beta',\alpha'}^b P_{\alpha'} P_{\alpha'} P_{\alpha} \hat{v}_{\alpha,\beta}^c P_{\beta} \rangle_{\beta}, \tag{D7}$$

in the language of quantum-state projector, where  $P_{\alpha} = |u_{\alpha}\rangle\langle u_{\alpha}|$  and  $\langle ... \rangle_{\alpha}$  indicates  $\langle u_{\alpha}|...|u_{\alpha}\rangle$ . At this point, shift vector has been expressed as the derivative of a gauge-invariant quantity  $\mathcal{L}_{\beta\alpha}^{abc}(p)$ , which is suitable for numerical implementation, and corresponds to Eq. (6) in the main text.

Then, the first part of geometric part of  $\sigma^{abc}_{SC}(\boldsymbol{q},\omega)$  is

$$v_{\beta\alpha}^b v_{\alpha\beta}^c R_{\beta\alpha}^{b;a} = \hat{D}_p \mathcal{L}_{\beta\alpha}^{abc}(p) \tag{D8}$$

by noting that  $v_{\beta\alpha}^b v_{\alpha\beta}^c = \mathcal{L}_{\beta\alpha}^{abc}(p)$ .

Similarly, we can express the second part of geometric part of  $\sigma^{abc}_{\rm SC}(q,\omega)$  as

$$v_{\beta\alpha}^b v_{\alpha\beta}^c R_{\alpha\beta}^{c;a} = \hat{D}_p \mathcal{L}_{\alpha\beta}^{acb} (p). \tag{D9}$$

Finally, we obtain the geometric-loop formalism of photon-drag shift current photoconductivity:

$$\sigma_{\rm SC}^{abc}(\boldsymbol{q},\omega) = \frac{\pi e^3}{\hbar^2 \omega^2} \int [d\boldsymbol{k}] \sum_{n_{\alpha},n_{\beta}} f_{\alpha\beta} \delta(\omega_{\beta\alpha} - \omega) \left( \hat{D}_p \mathcal{L}_{\beta\alpha}^{abc}(p) - \hat{D}_p \mathcal{L}_{\alpha\beta}^{acb}(p) \right). \tag{D10}$$

It should be noted that the derivation in this section can be viewed as a generalization of the length-gauge Wilson-loop formulation of the conventional photogalvanic response [36]. Our geometric-loop approach instead works in the velocity gauge, explicitly reinstates the photon wavevector q, and recasts the response in terms of quantum-state projectors, yielding compact expressions with a transparent quantum-geometric interpretation.

#### E. Symmetry analysis for nonlinear photon-drag photoconductivity

In this section, we will discuss how the nonlinear photon-drag photoconductivity transforms under inversion  $\mathcal{P}$  and time reversal  $\mathcal{T}$ , and we will clarify the distinct behaviors of the  $q_{\text{even}}$  and  $q_{\text{odd}}$  contributions introduced in the main text. For spatial  $\mathcal{P}$  symmetry analysis is straightforward: odd-rank tensor components are  $\mathcal{P}$ -odd whereas even-rank tensor components are  $\mathcal{P}$ -even. By contrast,  $\mathcal{T}$  requires more care because current is dissipative and the response must be defined with a causal (retarded) prescription [6]. To keep track of causality, we write the frequency as  $\tilde{\omega} = \omega + i/\tau$  (with  $\tau$  the relaxation time) and use  $\tilde{\omega}$  as the argument of the response functions. With this convention, the second-order photon-drag current is written as:

$$J^{a,(2)}(\boldsymbol{q},\tilde{\omega}) = \sigma^{abc}(\boldsymbol{q},\tilde{\omega})E_b(\tilde{\omega})E_c(-\tilde{\omega}). \tag{E1}$$

The time-reversal counterpart of Eq.(E1) is

$$J'^{(a,(2)}(\boldsymbol{q},\tilde{\omega}) = \sigma'^{abc}(\boldsymbol{q},\tilde{\omega})E'_b(\tilde{\omega})E'_c(-\tilde{\omega}). \tag{E2}$$

Under  $\mathcal{T}$ , we have:  $J^a(\boldsymbol{q}, \tilde{\omega}) \rightarrow J'^{,a}(\boldsymbol{q}, \tilde{\omega}) = -J^a(-\boldsymbol{q}, -\tilde{\omega})$  and  $E_a(\tilde{\omega}) \rightarrow E'^{,a}(\tilde{\omega}) = E^a(-\tilde{\omega})$ , then Eq.(E2) can be further written as

$$-J^{a}(-\boldsymbol{q}, -\tilde{\omega}) = \sigma'^{abc}(\boldsymbol{q}, \tilde{\omega}) E_{b}(-\tilde{\omega}) E_{c}(\tilde{\omega}). \tag{E3}$$

Meanwhile, we can rewrite Eq.(E1) as

$$J^{a,(2)}(-\boldsymbol{q}, -\tilde{\omega}) = \sigma^{abc}(-\boldsymbol{q}, -\tilde{\omega})E_b(-\tilde{\omega})E_c(\tilde{\omega}). \tag{E4}$$

Comparing Eq.(E4) to Eq.(E3), we conclude that  $\mathcal{T}$  requires the photoconductivity to transform as follows:

$$\sigma^{\prime,abc}(\boldsymbol{q},\tilde{\omega}) = -\sigma^{abc}(-\boldsymbol{q},-\tilde{\omega}). \tag{E5}$$

Let's take photoconductivity of linear photon-drag injection current  $\sigma^{abc}_{IC,L}(q,\tilde{\omega})$  as the example to illustrate how to use Eq.(E5) to analyze the behavior of photoconductivity under  $\mathcal{T}$ . According to Eq.(B5), the microscopic expression for  $\sigma^{abc}_{IC,L}$  is given by

$$\sigma_{\rm IC,L}^{abc}(\boldsymbol{q},\omega) = \frac{2e^3}{\hbar^2\omega^2} \int [d\boldsymbol{k}] \sum_{n_\alpha,n_\beta} \frac{f_{\alpha\beta}}{(\omega_{\beta\alpha} - \omega)^2 + \tau^{-2}} \operatorname{Re}\{v_{\beta\alpha}^b v_{\alpha\beta}^c\} \left(v_{\beta\beta}^a - v_{\alpha\alpha}^a\right). \tag{E6}$$

where we explicitly show the relaxation time dependence of Dirac delta function. According to Eq. (E5), we have

$$\sigma_{\rm IC,L}^{\prime,abc}(\boldsymbol{q},\omega) = -\frac{2e^3}{\hbar^2\omega^2} \int [d\boldsymbol{k}] \sum_{\boldsymbol{n}=n_0} \frac{f_{\beta\alpha}}{(\omega_{\alpha\beta} + \omega)^2 + (-\tau)^{-2}} \operatorname{Re}\{v_{\alpha\beta}^b v_{\beta\alpha}^c\} \left(v_{\alpha\alpha}^a - v_{\beta\beta}^a\right) = -\sigma_{\rm IC,L}^{abc}(\boldsymbol{q},\omega), \tag{E7}$$

where index exchange  $\alpha \leftrightarrow \beta$  in the first equality indicates  $\mathbf{q} \to -\mathbf{q}$ . Other photoconductivity can be analyzed in a similar way. In summary, we have:

$$\sigma_{\rm IC,L}^{\prime,abc}(\boldsymbol{q},\omega) = -\sigma_{\rm IC,L}^{abc}(\boldsymbol{q},\omega), \ \sigma_{\rm IC,C}^{\prime,abc}(\boldsymbol{q},\omega) = \sigma_{\rm IC,C}^{abc}(\boldsymbol{q},\omega)$$
 (E8)

and

$$\sigma_{\rm SC,L}^{\prime,abc}(\boldsymbol{q},\omega) = \sigma_{\rm SC,L}^{abc}(\boldsymbol{q},\omega), \ \sigma_{\rm SC,C}^{\prime,abc}(\boldsymbol{q},\omega) = -\sigma_{\rm SC,C}^{abc}(\boldsymbol{q},\omega). \tag{E9}$$

Having established how the photoconductivity transforms when both the system and the optical wavevector  $\mathbf{q}$  are acted on by  $\mathcal{T}$ , we now hold  $\mathbf{q}$  fixed (treating it as an external parameter) and examine the transformation under  $\mathcal{T}$  acting on the system alone. To this end, we expand the photoconductivity in powers of  $\mathbf{q}$ :

$$\sigma^{abc}(\boldsymbol{q},\omega) = \sigma^{abc}(\omega) + q_d \sigma^{abcd}(\omega) + q_d q_e \sigma^{abcde}(\omega) + \cdots$$
 (E10)

Since q is odd under  $\mathcal{T}$ ,  $q_{\text{even}}$  and  $q_{\text{odd}}$  contributions of photoconductivity are expected to transform differently. Thus, we separate  $\sigma^{abc}(q,\omega)$  as

$$\sigma^{abc}(\boldsymbol{q},\omega) = \sigma^{abc}(\boldsymbol{q}_{\text{even}},\omega) + \sigma^{abc}(\boldsymbol{q}_{\text{odd}},\omega). \tag{E11}$$

From Eq. (E8) and Eq. (E9), we directly find that

$$\sigma_{\rm IC,L}^{\prime\prime,abc}(\boldsymbol{q}_{\rm even},\omega) = -\sigma_{\rm IC,L}^{abc}(\boldsymbol{q}_{\rm even},\omega), \ \sigma_{\rm IC,L}^{\prime\prime,abc}(\boldsymbol{q}_{\rm odd},\omega) = \sigma_{\rm IC,L}^{abc}(\boldsymbol{q}_{\rm odd},\omega), 
\sigma_{\rm IC,C}^{\prime\prime,abc}(\boldsymbol{q}_{\rm even},\omega) = \sigma_{\rm IC,C}^{abc}(\boldsymbol{q}_{\rm even},\omega), \ \sigma_{\rm IC,C}^{\prime\prime,abc}(\boldsymbol{q}_{\rm odd},\omega) = -\sigma_{\rm IC,C}^{abc}(\boldsymbol{q}_{\rm odd},\omega)$$
(E12)

and

$$\sigma_{\text{SC,L}}^{\prime\prime,abc}(\boldsymbol{q}_{\text{even}},\omega) = \sigma_{\text{SC,L}}^{abc}(\boldsymbol{q}_{\text{even}},\omega), \quad \sigma_{\text{SC,L}}^{\prime\prime,abc}(\boldsymbol{q}_{\text{odd}},\omega) = -\sigma_{\text{SC,L}}^{abc}(\boldsymbol{q}_{\text{odd}},\omega), \\
\sigma_{\text{SC,C}}^{\prime\prime,abc}(\boldsymbol{q}_{\text{even}},\omega) = -\sigma_{\text{SC,C}}^{abc}(\boldsymbol{q}_{\text{even}},\omega), \quad \sigma_{\text{SC,C}}^{\prime\prime,abc}(\boldsymbol{q}_{\text{odd}},\omega) = \sigma_{\text{SC,C}}^{abc}(\boldsymbol{q}_{\text{odd}},\omega),$$
(E13)

where superscript " indicate that only the system is transformed under  $\mathcal{T}$ . By combining the transformation properties under  $\mathcal{P}$  of the  $q_{\text{even}}$  and  $q_{\text{odd}}$  contributions, we obtain the results summarized in Table I.

# F. Continuum-model band structures of twisted bilayer graphene

In this section, we present the low-energy band structures of TBG discussed in the main text. Fig. S1 shows the low-energy band structures of TBG computed from the relaxed continuum model along the high-symmetry path K- $\Gamma$ -M-K. Panels (a-c) display the centrosymmetric case at twist angles  $\theta = 1.05^{\circ}$ ,  $1.15^{\circ}$ , and  $1.25^{\circ}$ . At  $\theta = 1.05^{\circ}$ , slightly above the magic angle, the bands are the flattest; with increasing  $\theta$  the moiré bandwidths broaden progressively, shifting spectral features to higher energies. Energies are measured in meV relative to charge neutrality. Panel (d) shows the low-energy bands with inversion breaking at  $\theta = 1.05^{\circ}$ . Introducing a sublattice-staggered potential  $\pm \delta_S$  with  $\delta_S = 0.02$  eV lifts the K-point degeneracy and opens a gap, thereby driving a semimetal-to-semiconductor transition.

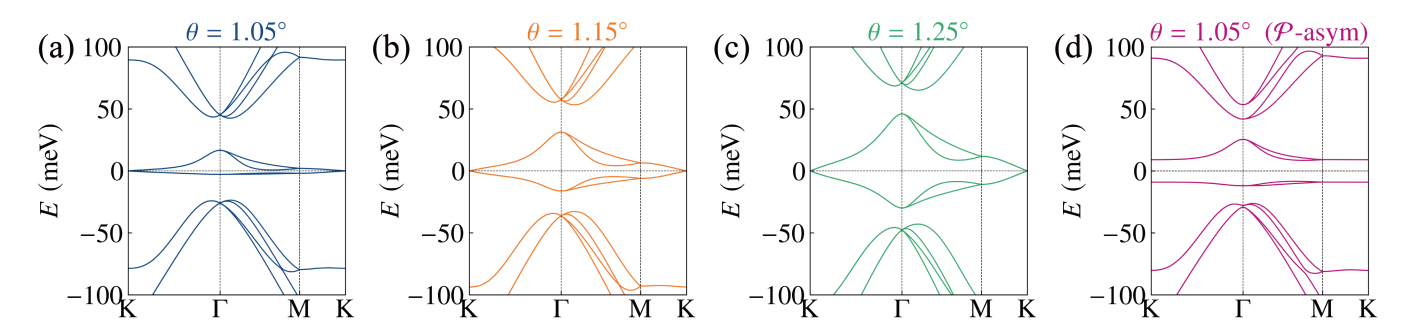


FIG. S1. Band structures from the relaxed continuum model of twisted bilayer graphene along  $K-\Gamma-M-K$ . (a-c) Centrosymmetric TBG at twist angles  $\theta = 1.05^{\circ}$ ,  $1.25^{\circ}$ , and  $1.15^{\circ}$ , respectively. (d) Inversion-broken case at  $\theta = 1.05^{\circ}$ .